Desalination and Water Treatment
www.deswater.com

doi:10.5004/dwt.2018.22536

120 (2018) 289–303
July

Reductive degradation of high concentration nitrobenzene using nanoscale zero-valent iron particles immobilized on Polyaniline

Samaneh Dehghan[a], Ali Azari[b], Roshanak Rezaei Kalantary[c,*]

[a]*Student Research Committee, Faculty of Public Health, Iran University of Medical Sciences, Tehran, Iran*
[b]*Department of Environmental Health Engineering, School of Public Health, Tehran University of Medical Sciences, Tehran, Iran*
[c]*Research Center for Environmental Health Technology (RCEHT), Iran University of Medical Sciences, Tehran, Iran,*
Tel. +98 9123234586, email: rezaei.r@iums.ac.ir (R.R. Kalantary)

Received 11 January 2018; Accepted 20 May 2018

ABSTRACT

In this paper, we focused on the development, characterization and application of magnetic polyaniline/nanozero-valent iron composite nanofibers (PANI/NZVI CNFs), as a nano-degrading agent. An economical and efficient approach was used for green synthesis of the PANI/NZVI CNFs for nitrobenzene (NB) degradation. A response surface methodology (RSM) was used to investigate the impact of experimental factors like pH, NB concentration and PANI/NZVI CNFs dosage) on the degradation of NB using the PANI/NZVI CNFs. Also, the Box-Behnken design (BBD), based on RSM, was used to optimize the variables such as solution pH (2.0–10.0), initial NB concentration (40–200 mg/L), and PANI/NZVI CNFs dosage (0.25–1.5 g/L). ANOVA analysis revealed that key variables were interaction between initial NB concentration, PANI/NZVI CNFs dosage and pH in quadratic term. The statistical analysis showed that PANI/NZVI CNFs dosage had a synergistic effect, whereas pH and NB concentrations had an antagonistic impact on degradation rate. High removal efficiency (>98%) was obtained under the optimal conditions (pH: 2, NB concentration.: 40 mg/L and PANI/NZVI CNFs dose 0.88 g/l). The analytical results of the GC/MS analysis identified that aniline, nitrosobenzene, phenyl hydroxylamine, azobenzene, and azoxybenzene were probably the main intermediate products of the NB degradation using PANI/NZVI CNFs.

Keywords: Nitrobenzene; Degradation, PANI/NZVI CNFs;Response surface methodology, Mechanism

1. Introduction

Nitrobenzene ($C_6H_5NO_2$, NB), as a type of chemical material, has been known as an important groundwater pollutant, because of the extensive utilization in national defense, pharmacy, dyeing and other industries [1]. It is also utilized as an essential substance in synthetic fuels, detergents, rubber, explosives, and the other materials; as a result, large quantities of waste materials are released into the environmental resources [2–5]. According to the literature, the annual rate of NB released into soil and water resources is over 8.6 million kilograms [6]. It is known as a highly toxic and recalcitrant organic contaminant, with stable chemical structure. NB, even at low concentrations, can harm the reproductive system of rodents and may lead to the critical dangers to the environment, organisms and the human life beings [7,8]. NB has been listed as a priority control pollutant in lots of countries because of its teratogenic, carcinogenic and mutagenic impacts. Moreover, the World Health Organization (WHO) has classified it as an animal carcinogenic substance. Therefore, removal of NB from wastes/wastewater is very important [7,9]. In China, the NB concentrations of industrial wastewater discharge (GB8978-1996) and surface water environmental quality standard (GB3838-2002) are < 2.0 and 0.017 mg/L, respectively [2]. In the past few decades, a variety of environmental remediation techniques have been applied for NB removal including ozonation, oxidation in supercritical water, photocatalysis and modified Fenton reaction [10]. Traditional remediation approaches, like pump-and-

---

*Corresponding author.

treat and penetrable reactive barrier walls, widely depend on dense non-aqueous phase liquids (DNAPLs) dissolution and transport for treatment; thus, their efficiency is not favorable [1]. NB is comparatively resistant against biodegradation, because of the existence of strong electron-withdrawing nitro-group in its structure which greatly decreases the electronic cloud density to strongly fix the chemical properties [9]. Zero-valent iron (ZVI) has been extensively applied for removal of nitrocompounds containing amido materials as the principal reductive substances that are able to be biodegraded quickly. NB could be only partly reduced to aniline, with nitrosobenzene as an intermediate product or azobenzene as by-products because of the high particle size and low reactivity of micro-scale ZVI,. Hence, there is a widespread enthusiasm for application of nanoscale ZVI (NZVI), due to its high specific surface area to volume ratio, higher reactivity and special physical and chemical characterizations, which can efficiently convert NB nitro into amino; as a result, the toxicity of NB decreases and its biodegradable properties increase [11]. Unlike other remediation approaches such as adsorption, air stripping and biotransformation process, NZVI contains different specific benefits like mild reaction condition, rapid reaction rate, low preparation costs. It is a green process technology and chemical additives are not added [12]. In addition, it can be applied as an efficient reductant catalyst to remove a large number of reducible pollutants like chlorinated organic compounds, nitrate, heavy metal ions and oxoanion, trichloroethylene, nitroaromatics, pesticides, chlorinated methanes, decabrominated diphenyl ether and organic-solvents [13]. Furthermore, regarding the magnetic properties of PANI/NZVI CNFs (which is related to the presence of NZVI in composite structure), the cost and time of separation decrease and lead to easy and rapid separation from aqueous solution via an external magnetic field [14]. In the study by Peng et al. (2017), NZVI/biochar composite was used for p-itrophenol (PNP) removal in aerobic or anaerobic conditions and the results showed that PNP removal rate in the acidic conditions was higher than that of alkali conditions, especially at pH 9.0. [15]. In another research by Tang et al., nanoscale zero-valent iron particles supported on mesoporous silica (NZVI/SBA-15) were prepared for degradation of p-nitrophenol (PNP). Batch experiments results showed that when solution pH increased from 3.0 to 9.0, PNP degradation decreased from 96.70 to 16.14%, respectively. Furthermore, degradation equilibrium was reached within 5 min, which was initial PNP concentration- independent [16].

Even though NZVI is commonly used as a remediation agent for pollutant removal, lots of critical challenges have been present in their application in either experimental or field scales. In this study, it was found that the optimum pH value for NB degradation using NZVI was 3.0; and, in the absence of surface protection, freshly prepared NZVI showed a tendency to be aggregated into large clusters [10,12]. The aggregation of iron nanoparticles will cause negative effects on their reactivity and mobility. Also, NZVI is susceptible for oxidizing, due to high reactivity that drops the reduction rate because of the creation of oxide layers blocking the serviceable active surface sites. Thus, controlling the aggregation and oxidation of NZVI is the main concern [12]. Therefore, for overcoming these difficulties, a wide number of researches have focused on NZVI surface modification using supporting materials [13]. The obtained findings of various researches have demonstrated that the modified NZVI on various supporting substances caused an enhancement in their dispersion, stability, and reactivity [2]. The supporting materials include polymeric resin, PVA, activated carbon, zeolite, metal oxides and bauxite [13]. However, the transport of pollutants to reactive nanoparticles has somehow restricted because of the dense structure of solid support [17]. In recent years, conducting polymer nanostructures have attracted a special attention in the fields of nanoscience and nanotechnology, due to their unique combination of the electronic properties of conductive polymers and the large surface area of nanomaterials. Among dimensional conducting polymer nanostructures, nanofibers of polyaniline (PANI) have stimulated research interests as they can be easily synthesized in bulk quantities and have a large surface area to volume ratio [18–20]. Sharma et al. (2014) synthesized nanocomposite polyaniline zirconium(IV) selenotungsto phosphate for the separation of toxic metal ions and the results showed that this nanocomposite has an excellent ion exchange capacity (1.20 meq g^{-1}) along with high thermal stability [21]. Moreover, Naushad et al. (2013) used polyaniline Sn(IV) silicate composite for adsorption of cadmium ion. Adsorption properties of different metal ions have been investigated and the results have revealed that polyaniline Sn(IV) silicate has the highest adsorption capacity for Cd^{2+}ion [22].

PANI, with good redox properties, high suspension ability, low-dimensional system, high conductivity and excellent environmental stability, can provide a superior performance for potential applications in sensors, actuators, super capacitors, field effect transistors and in separation or purification systems [18,23]. On the other hand, Colak et al. reported that iron samples coated with PANI exhibit much better protection against corrosion in acidic conditions than the polypyrrole-coated ones [24]. Thus, in this study, a novel magnetic polyaniline/nano zero valent iron composite nanofibers (PANI/NZVI CNF_s), as a nano-degrading agent for NB removal and a model organic pollutant, was successfully synthesized using the PANI nanofibers as support matrix and the polymerization by-products $FeCl_2$/ $FeCl_3$ as a source of NZVI, under borohydride reduction, at room temperature [23]. Since NB has hazardous nature, high toxicity and harmful effects on public health, it has also been well-known. Numerous studies have reported that PANI/Fe has been used as an adsorbent, but there are few studies on the reductive degradation of NB in aqueous solution using PANI/NZVI CNFs [25].

As an alternative to specify the optimum operating conditions for the removal of NB, response surface methodology (RSM) was used in the current research [26]. The majority of conventional studies vary one factor at a time and other parameters remain unchanged for the optimization of process variables, which is time-consuming and difficult to predict the true optimum and interactions among different parameters and also increases the number of required experiments. As an alternative method, Box-Behnken design (BBD) based on response surface methodology (RSM) could overcome these above-mentioned defects [27,28]. The statistical experimental design is an effective and powerful method for screening key factors and concurrent optimization of process factors [29]. It determines the individual and interaction effects of independent variables (x_1, x_2… x_k) on the response (y) by generating a mathematical model. Three factors: initial concentration of NB, concentration of PANI/NZVI CNFs, and pH are selected as independent variables influencing the reduction process [30]. Therefore, the present work focuses on (i) synthesis and physicochemical characterization of PANI/NZVI CNFs, (ii) comparison of NB removal behaviors of PANI, NZVI and PANI/NZVI CNFs, (iii) evaluation of the removal of NB under various parameters of process, and (iv) kinetics and possible mechanistic pathway of NB removal using PANI/NZVI CNFs [23,31].

2. Material and methods

2.1. Materials and chemicals

Aniline monomer (ANI, purity 99%) was purchased from Merck Co. (Germany) and purified by vacuum distillation prior to use and distilled ANI was kept in a refrigerator before using for polymerization. Nitrobenzene ($C_6H_5NO_2$, 99%), anhydrous iron chloride ($FeCl_3$, 97%), sodium borohydride ($NaBH_4$, 98%), hydrochloric acid (HCl, 37%), sodium hydroxide (NaOH, 98%) and the other chemical substances were prepared from Sigma Aldrich (St. Louis, MO, USA). It should be noted that all the chemicals used in this study were of analytical grade. Ultrapure water was used to prepare all experimental solutions and polymerization media.

2.2. Preparation of PANI nanofibers and PANI/NZVI

2.2.1. Preparation of PANI nanofibers

The rapid-mixing polymerization approach was applied for synthesis of PANI NFs at room temperature. In a common polymerization process, 6 g iron chloride (III), as an oxidant agent, was dissolved in 80 ml double distilled water in a 250-ml Erlenmeyer flask. In order to prevent secondary growth of PANI, Aniline (ANI) monomer (0.8 ml) was syringed all at the same time to the oxidant solution with sufficient (600 rpm) stirring to evenly distribute the oxidant and monomer molecules for 5 min. Then, the reaction mixture was kept in quiescent conditions for 2 d. Finally, the resulted polymer (PANI) was filtered, rinsed via water and acetone, and dried at 60°C [18].

2.2.2. Synthesis of PANI/NZVI CNF$_s$

In order to synthesize PANI/NZVI CNFs, the prepared PANI NFs (without removing them from the polymerization medium) were applied as a supporting material ($FeCl_2$ and/or any remaining $FeCl_3$) and the source of NZVI. The mixture of polymerization (PANI NFs and $FeCl_2$/$FeCl_3$) was stirred mechanically under N_2 gas for supporting NZVI on the PANI NFs. Some drops of freshly prepared 1 M sodium borohydride ($NaBH_4$) solution was added slowly to the mixture including PANI NFs that caused the creation of NZVI on the PANI NFs matrix. For completion of the reduction of the Fe source, the mixture was stirred for another 20 min. The produced PANI/NZVI CNFs were magnetically separated, rinsed sequentially via water and ethanol and finally dried at 60°C [18]. The synthesis process of PANI NFs and PANI/NZVI CNFs has been shown in Fig. 1.

2.3. PANI/NZVI CNFs characterization

An Auriga field emission scanning electron microscope (FE-SEM; Carl Zeiss, Germany) and a JEOL JEM-2100 high resolution transmission electron microscope (HR-TEM; JEOL, Japan) were used to study the surfaces and morphological features of PANI NFs and PANI/NZVI CNFs. A JEOL JEM-2100 HR-TEM instrument with a LaB6 filament operated at 200 kV was also applied for taking the TEM images. HR-TEM samples were obtained via putting a drop of sample suspension in 2-propanol on a copper grid. The specific surface areas (The Brunauer–Emmett–Teller (BET)) of the nano-NZVI, PANI nanofibers and PANI/NZVI CNFs were determined via a low temperature N_2 adsorption-desorption approach by means of a Micromeritics ASAP 2020 gas adsorption apparatus (USA). X-ray diffraction (XRD) pattern of the PANI/NZVI CNFs was carried out via an X-ray powder diffractometer with Cu anode (PAN alytical Co. X'pert PRO, UK), running at 40 kV and 30 mA, scanning from 10–80° at a scan speed of 1°/min. An attenuated total reflectance-fourier transform infrared (ATR-FTIR) spectrum 100 spectrometer (Perkin-Elmer, USA), with a germanium crystal, was applied for recording the IR spectrum of PANI/NZVI CNFs. For IR measurement, the frequency range, resolution and number of scans were 600–2000 cm^{-1}, 4 cm^{-1} and 10, respectively. X-ray photoelectron spectroscopy (XPS),

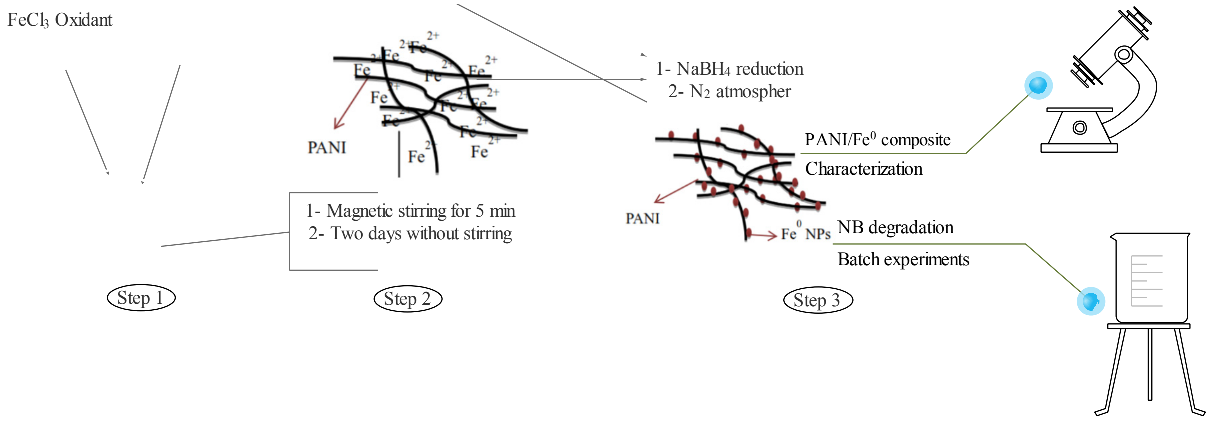

Fig. 1. Schematic representation for the preparation of PANI/NZVI CNFs.

Perkin Elmer PHI 5500 XPS system on a Kratos Axis Ultra device, with an Al monochromatic X-ray source (1486.6 eV), was applied to find the oxidation statues of the present elements in the structure of PANI/NZVI CNFs. XPS curve fitting and background subtraction were accomplished using XPS PEAK 41 software. For analysis of Fe content in the PANI/NZVI CNFs, the PANI/NZVI CNF$_s$ was digested with 2M HCl. The magnetic properties of the PANI/NZVI CNFs were recorded using a vibrating sample magnetometer (VSM, MDKFD, Iran) at room temperature.

2.4. Batch experiments of NB degradation

NB stock solution (1000 mg/L) was obtained via addition of 83.3 µl NB in 0.1 L ultrapure water and the batch experiments were carried out at room temperature. The experiments conducted by adding different amounts of the PANI/NZVI CNFs into 50 ml solution with initial concentrations of 40–200 mg/L NB at various pH values, according to the designed runs by the RSM approach. The mixture was agitated at 200 rpm with a magnetic stirrer in the constant time of 45 min, based on the related articles [32–34]. The solution pH was set using 0.1 N NaOH and 0.1 N HCl solutions. All experiments were performed in duplicate and the average values were reported to ensure the reliability of the results. NB concentrations in both initial and residual samples were analyzed using an Agilent 1100 Series HPLC system (Agilent Technologies, Santa Clara, CA) equipped with a C18 column (5 µm × 3.9 × 150 mm) and a diode array ultraviolet detector. The methanol/water mixture with the ratio of 50/50 was selected as a mobile phase at a flow rate of 1 ml·min^{-1} for 15 min. The volume of injection was 20 µl and detection absorbance was monitored at 254 nm. The NB degradation efficiency (% removal) was determined using the following equation:

$$\%\ \text{Removal} = \frac{C_0 - C_t}{C_0} \times 100 \tag{1}$$

where C_0 and C_t (mg/L) are the initial and residual NB concentrations, respectively. The Gas chromatography-mass spectrometric analyses system (Agilent technologies 7890 A GC system) was used to identify the final by-products of NB degradation.

2.5. Statistical analysis of the experimental design

The Box Behnken design (BBD) is a combination of statistical and mathematical methods for optimization of a process [28]. Response surface methodology (RSM) based on BBD was used in order to optimize the experimental factors and obtain the least number of experiments. This decrease in the number of experiments leads to a decrease in the cost of required materials, time and laboratory works [35]. Such statistical approach also provides valuable information on possible interactions between the variables and responses. RSM-based BBD requires an experimental number, given by the formula $N = 2k(k - 1) + C_0$, where k and C_0 are the number of factors and central point, respectively. All parameters are studied in three levels: –1, 0, +1 [11]. For finding the role of experimental factors on the degradation efficiency, the effect of three main factors including initial NB concentration (mg L^{-1}), CNF$_s$ dosage (g L^{-1}) and solution pH was investigated. The experimental ranges and the levels of the operational variables have been presented in Table 1. The design package experiment 7 (Stat-Ease Inc., Minneapolis MN, USA) was applied for regression analysis of the experimental results. The analysis of variance (ANOVA) was used in order to confirm equation for determining the fitness of each coefficient and estimation of goodness of fit of each term. To evaluate the fitness of the model, coefficient of determination (R^2) was used. F-test was also applied for evaluating the significance of the statistics of the model equation.

$$Y = \beta_0 + \sum_{i=1} n\beta_i X_i + \sum_{i=1} n\beta_{ii} X_i^2 + \sum_{i=1} n\beta_{ij} X_i X_j + \ldots + e \tag{2}$$

where, Y is NB reduction efficiency, β_0 is intercept, β_i is linear coefficient, β_{ii} is the quadratic coefficient, β_{ij} is the interaction coefficients, n is the number of independent variables, X is the independent factors and e is the random error [30]. Table 1 shows the ranges and levels of each experimental factors. Also, ANOVA results of the quadratic models for the percentage of NB removal have been shown in Table 2.

Table 1
Experimental ranges and levels of the operational variables

Variables	Symbols	Units	Level (coded value)		
			–1	0	+1
pH	X_1	–	10	6	2
NB Conc.	X_2	mg/L	200	120	40
CNFs Dose	X_3	g/L	1.5	0.88	0.25

Table 2
Results of the BBD experiment in NB removal

Run	pH	NB Conc.	CNF$_s$ Dose	Actual NB removal (%)	Predicted NB removal
1	6.00	120.00	0.88	75	76.21
2	2.00	120.00	1.50	90.12	92.13
3	2.00	40.00	0.88	98.2	97.6
4	6.00	40.00	0.25	61.11	62.2
5	6.00	120.00	0.88	65.34	66.12
6	10.00	120.00	0.25	55	55.7
7	10.00	120.00	1.50	65	67.11
8	2.00	120.00	0.25	66.33	65.61
9	10.00	200.00	0.88	52	52.2
10	6.00	120.00	0.88	63.77	63.24
11	6.00	200.00	1.50	60.39	59.3
12	6.00	120.00	0.88	60.4	61.06
13	2.00	200.00	0.88	68.06	69.35
14	6.00	40.00	1.50	80.89	82.78
15	10.00	40.00	0.88	73	75.03
16	6.00	200.00	0.25	53.51	55.36
17	6.00	120.00	0.88	78.31	77.24

Each independent variable (X_i) was converted to coded values, according to Eq. (3):

$$A_i = \frac{X_i - X_m}{\Delta x} \tag{3}$$

where A_i is the coded value of each factor, X_0 is the real value of each factor in the central point and ΔX refers to the half of the difference between the upper and lower values of the independent variable.

3. Theory/calculation

In this paper, the development, characterization and application of the magnetic PANI/NZVI CNFs, as a degradation agent for NB removal has been done and RSM was used for investigation of the influence of the experimental factors (like pH, NB concentration, PANI/NZVI CNFs dosage) on the degradation process. The findings showed that RSM with a Box Behnken design could be considered as an efficient approach to model and optimize the experimental factors.

4. Result and discussion

4.1. Characterization of the PANI/NZVI CNFs

4.1.1 Scanning electron microscopy (SEM)

The SEM images of PANI NFs, which were prepared by the rapid mixing method, and PANI/NZVI CNFs have been illustrated in Figs. 2a and b. Accordingly, the synthesized PANI NFs was 30–50 nm in diameter, with smooth surfaces which have high inclination to be agglomerated into an interconnected nanofiber network. After the modification of the NZVI particles, a slight increase was observed in PANI NFs diameter to 50–80 nm showing rougher surface than pure PANI. These results are similar to SEM images of PANI/Fe^0 which were done by Bhaumik et al. and Piao et al. [18,23,36].

4.1.2. Transmission electron microscopy (TEM)

TEM images of the PANI and PANI/NZVI CNFs at two different magnifications (10K×, 200K×) have been represented in Figs. 3a–c, respectively. Based on the presented TEM images, the pure PANI NFs were prepared by the interfacial polymerization products which have 30–50 nm particle diameter. The undoped polymer had a loamy structure, but the structure of doped samples became scalier, finally leading to the appearance of small black islands. At the beginning of the polymerization process, clean nanofibers were produced with 30–50 nm average diameters. However, in the following steps, they became coarse and the last obtained nanofiber materials were created in agglomerated forms with irregular shapes (Fig. 3a). The obtained findings implied that the initial produced nanofibers can play the role of scaffolds for the overgrowth of irregularly-shaped polyaniline. A closer observation (Fig. 3b) of PANI/NZVI CNFs reveals that NZVI with different grain sizes have easily been placed on PANI NFs surfaces. The darker parts of the image showed the presence of iron nanoparticles that have a relatively dense and uniform distribution. In this image, it was observed that the iron nanoparticles had a polygonal structure and were distributed non-uniform and interrelated in the surface and internal parts of PANI NFs.

4.1.3. X-ray diffraction (XRD) and Fourier transform microscopy (FTIR)

The XRD graphs of PANI NFs, PANI/NZVI CNFs and NZVI have been illustrated in Fig. 4a. Accordingly, a sharp

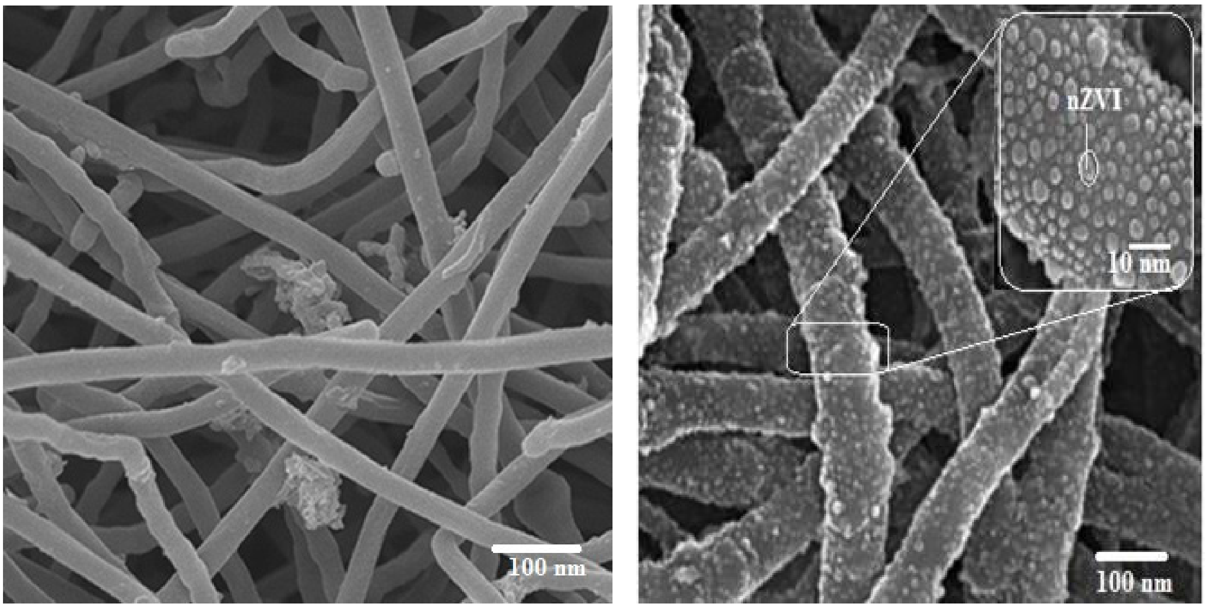

(a) (b)

Fig. 2. FE-SEM images of (a) PANI NFs (Magnification: 88.87K×) (b) PANI/NZVI CNFs (Magnification: 28.91K×).

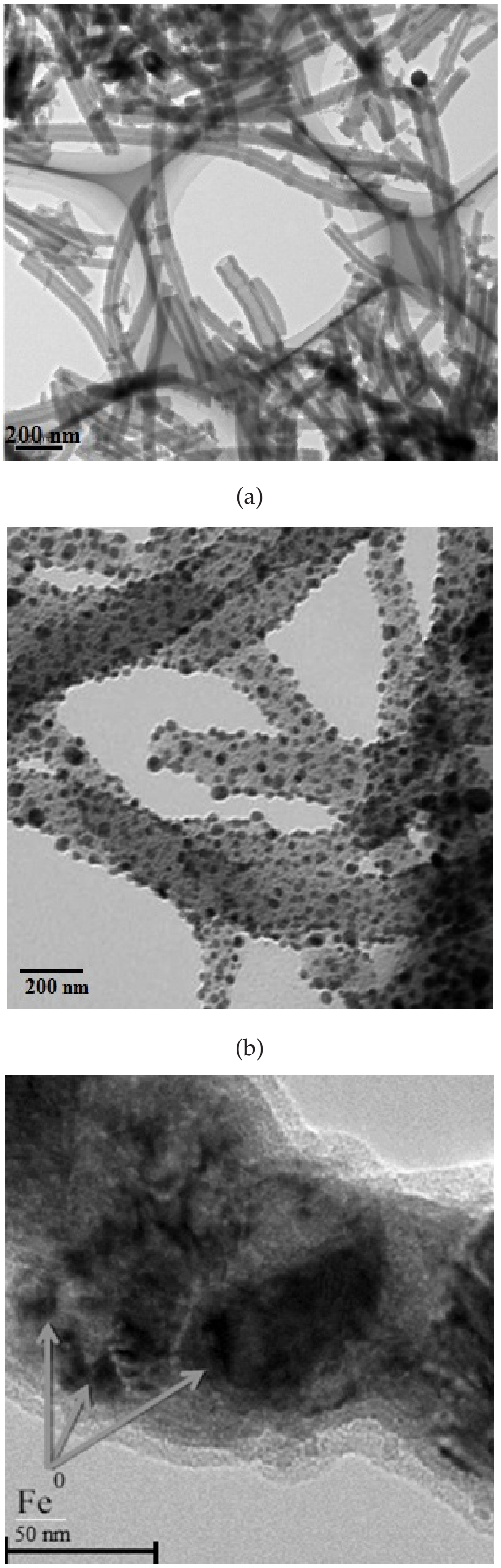

(a)

(b)

(c)

Fig. 3. HR-TEM images of (a) PANI NFs and PANI/NZVI CNFs at two different magnifications (b) (10K ×), (c) (200K×).

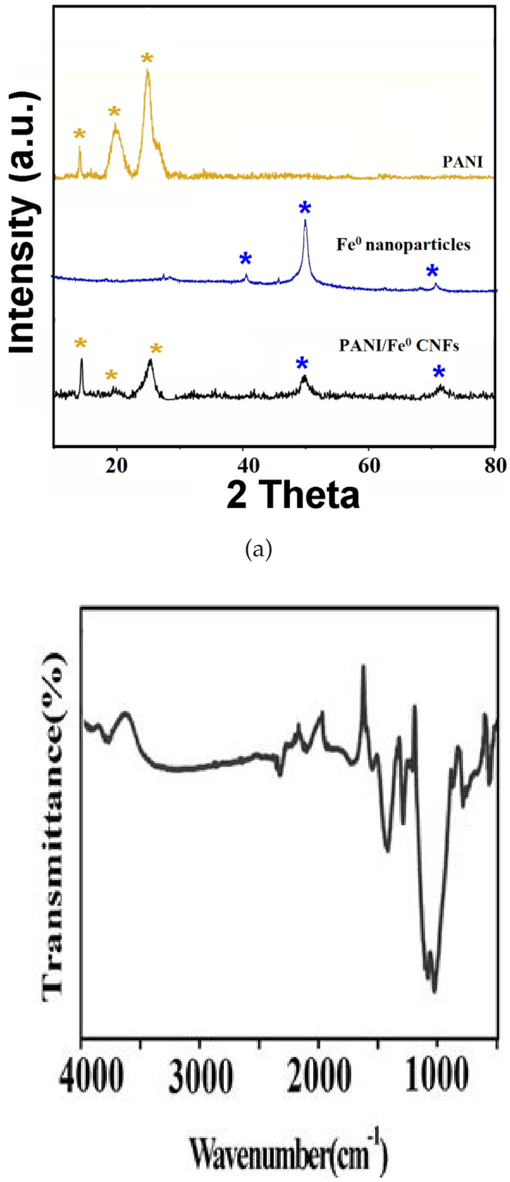

(a)

(b)

Fig. 4. (a) XRD pattern of the PANI, NZVI, PANI/NZVI CNFs and (b) ATR-FTIR spectrum of the PANI/NZVI CNFs.

peak is shown in XRD graphs of both PANI/NZVI CNFs and NZVI at $2\theta = 50.12°$ which reveals the presence of PANI in NZVI structure. However, in comparison with NZVI, a weaker and broader peak was observed at $2\theta = 50°$ in PANI/NZVI XRD graph, confirming the smaller particle size of PANI than NZVI. Furthermore, from the broad band at $2\theta = 25.34°$, it can be postulated that PANI has an amorphous structure. The FTIR spectroscopy is a very useful technique to understand the investigation of the structure and redistribution of elements, as well as the lattice vibrational modes [37,38]. The ATR-FTIR spectrum of the PANI/NZVI CNFs has been shown in Fig. 4b. The stretching bands at 1100 cm^{-1} are because of the stretching mode for the benzenoid ring and the band at 1219 cm^{-1} corresponds to C=N vibrational frequencies in Q–B–Q (quinonoid (Q) benzenoid (B) quinonoid rings of PANI NFs. The peaks at 1,670 cm^{-1} (OH bending vibration) indicated the presence of physiosorbed interstitial water molecules on the surface of NZVI. Besides, the broad and strong peaks were observed at about 3710 cm^{-1} (OH stretching vibration). The results of these analyses are in line with those of XRD and FTIR analyses on the Fe/PANI nanoparticles reported by other researchers [25,31].

4.1.4. X-ray photoelectron spectroscopy(XPS) and vibrating sample magnetometer (VSM) analyses

The N and Fe quantities and chemical states in PANI/NZVI CNFs were analysed using XPS analysis; based on the obtained results, around 4.75 and 26.89% of the synthesized catalyst were N and Fe, respectively. The N 1s (Fig. 5a) core spectrum of the PANI/NZVI CNFs could be fitted into three peaks with binding energies centered at 398.2 eV, 399.1 eV and 400.1 eV corresponding to quinonoid imine (=N–) N, benzenoid amine (–NH–) N and the doped imine (–NH$^{+\cdot}$–) N, respectively. Furthermore, Fig. 5b shows the Fe 2p core level spectrum. The Fe2p spectrum could also be deconvoluted into the peaks centered at 710.45 eV and 712.62 eV, corresponding to the binding energies of Fe 2p3/2, while the peaks centered at 722.08 eV, 724.28 eV are associated with Fe 2p1/2 binding energies. The observed Fe2p peaks are in conformity with FeO, FeOOH and Fe_3O_4, which suggest that the NZVI nanoparticles deposited onto the PANI matrix were enclosed by a thin layer of iron oxides.

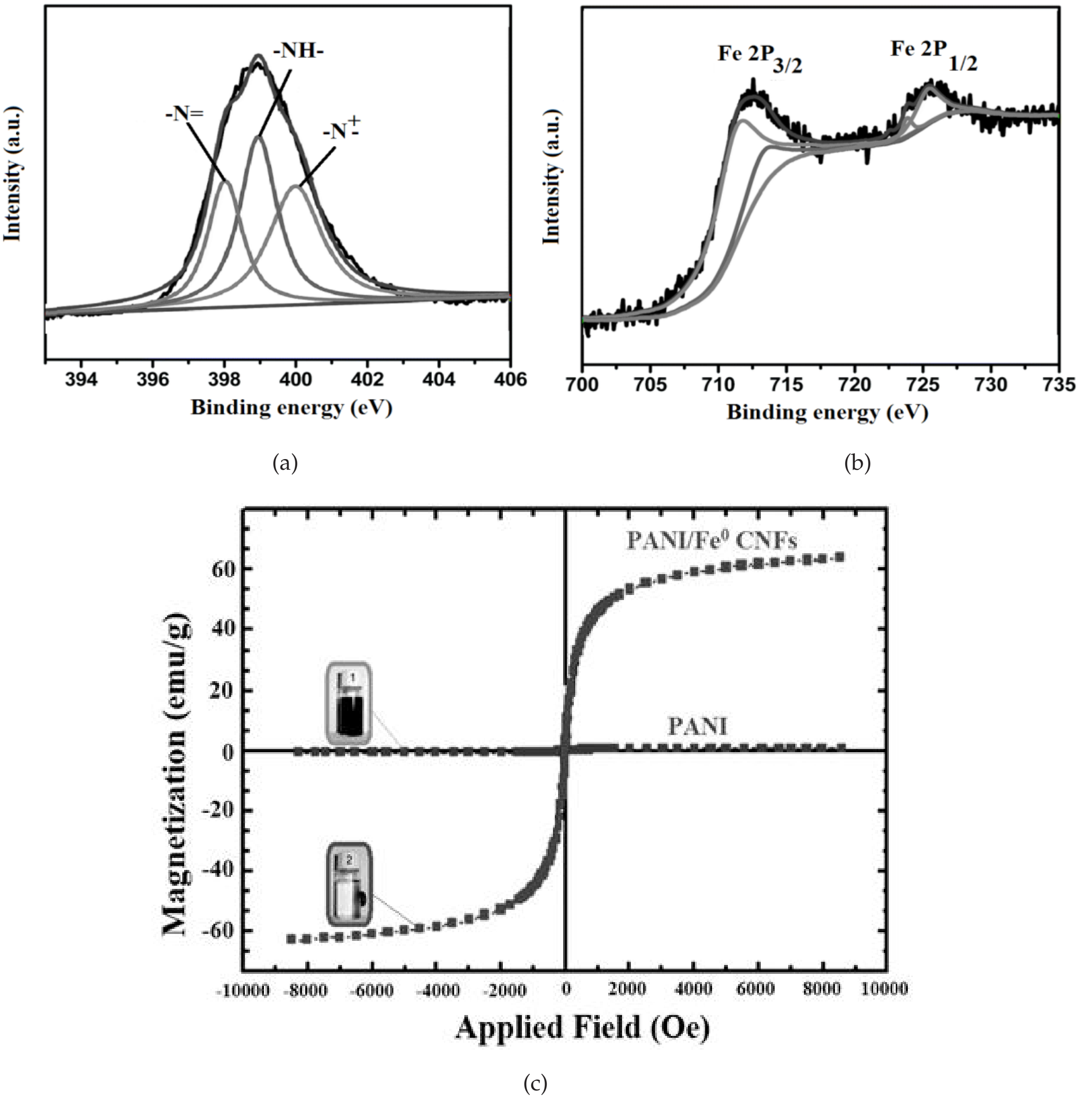

(a)

(b)

(c)

Fig. 5. (a) N 1s XPS spectrum of the PANI/NZVI CNFs, (b) Fe 2p XPS spectrum of the PANI/NZVI CNFs and (c) VSM image of the PANI/NZVI CNFs.

In addition, a very weak satellite peak at 706.36 eV, corresponding to NZVI $2p^{3/2}$, was hardly recognizable because of the large surface sensitivity (less than 10 nm in depth) of XPS. The magnetic characteristics of PANI/NZVI CNFs were studied not only to find the separation of adsorbent using an external magnet, but also to examine its regeneration after reaction with pollutants. Having a closer look to Fig. 5c, the magnetic hysteresis loop of PANI/NZVI CNFs was presented at room temperature. The specific saturation magnetization of PANI/NZVI CNFs was 65 emu/g, which guaranteed magnetic separation of CNFs.

The results of XPS of CNFs analysis are similar to those reported by Bhaumik et al. (2014 and 2015) and Piao (2015), but their magnetic properties of them are more than VSM analysis results [18,23,36].

4.2. Analysis of variance and fitting the quadratic model

A series of experiments were performed in a Box Behnken design (Table 3). Various statistical data (sum of squares of the errors, degree of freedom, mean square, F statistics and p value) were also obtained. The analysis of variance (ANOVA) confirms the adequacy of the studied model and the relationship between the experimental and predicted values. The model F-value and the corresponding P-value are 70.49 and <0.0001, respectively. The obtained findings showed that the applied model was statistically significant which can potentially be applied in order to predict responses. Values of "Prob>F" less than 0.05 confirm the significance of model terms. In addition, the most considerable factors and interaction effects have been shown in Table 3, which have a significant effect on the response parameters. In this case, A, B, C, AB, A^2 are significant model terms. Other model factors that their P-values are greater than 0.05 are not significant. The "Lack of Fit F-value" of 2.94 implies that this parameter is not significantly relative to the pure error. The "Pred R-Squared" of 0.87 has significant correlation with the "Adj R-Squared" of 0.98. "Adeq Precision" measures the signal to noise ratio. The ratio higher than 4 shows the desirability of the model. In this study, the obtained ratio was 27.90, confirming the adequate signal and the usability of the model to navigate the design space. The lower coefficient of variation (C.V% = 0.78) obviously demonstrated that the deviations between actual and predicted values were low confirming the precision and reliability of the conducted experiments.

The empirical relationship between the actual and predicted responses was explained via the second-order polynomial equation as follows:

$$\text{NB Degradation} = +54.46 - 23.96 * X_1 - 6.78 * X_2 + 4.43 * X_3 + 4.54 * X_1 * X_2 - 2.20 * X_1 * X_3 - 0.73 * X_2 * X_3 + 7.00 * X_1^2 - 0.89 * X_2^2 - 2.09 * X_3^2$$

X_1:pH , X_2:NB Conc., X_3:CNF$_s$ Dosage (4)

According to the above-mentioned equation, from the negative values of coefficients of the quadratic terms in the polynomial expression, it is obvious that these coefficients have a negative impact on the performance of nanocomposite. In Eq. (4), the sign (+) implies a direct relationship between the removal efficiency and the levels of the respective variables, while the sign (–) shows that removal efficiency declines in the presence of high levels. From the positive coefficients of the second-order model, it can be postulated that a synergistic relationship is dominated among the studied factors. But the negative coefficients

Table 3
Analysis of variance for efficiency (%)

Source	Sum of Squares	df	Mean Square	F -Value	p-value	
					Prob> F	
Model	5442.97	9	604.77	70.49	< 0.0001	significant
A-pH	4594.09	1	4594.09	535.45	< 0.0001	
B-NB Conc.	367.75	1	367.75	42.86	0.0003	
C- PANI/NZVI dosage	157.09	1	157.09	18.31	0.0037	
AB	82.26	1	82.26	9.59	0.0174	
AC	19.32	1	19.32	2.25	0.1772	
BC	2.10	1	2.10	0.25	0.6357	
A^2	206.21	1	206.21	24.03	0.0017	
B^2	3.33	1	3.33	0.39	0.5531	
C^2	18.42	1	18.42	2.15	0.1862	
Residual	60.06	7	8.58			
Lack of Fit	41.33	3	13.78	2.94	0.1621	not significant
Pure Error	18.73	4	4.68			
Cor Total	5503.03	16				
Std. Dev.	2.93		R-Squared	0.99		
Mean	56.35		Adj R-Squared	0.98		
C.V. %	0.78		Pred R-squared	0.87		
PRESS	690.53		Adeq precision	27.90		

showed the antagonistic effect of variables on the response factors. The importance of each individual factor as well as interactions mainly depends on the coefficient in the equation. For example, it is obvious that pH has a critical influence on NB degradation.

After deleting the non-significant factors, the quadratic regression equation of RSM was simplified as follows:

$$\text{NB Degradation} = +54.46 - 23.96 * X_1 - 6.78 * X_2 + 4.43 * X_3 + 4.54 * X_1 * X_2 + 7.00 * X_1^2 \quad (5)$$

4.3. Effect of operational variables (pH, initial NB concentrations and PANI/NZVI CNFs dosages)

It is worthwhile to mention that solution pH is one of the most considerable agents in the degradation of surface features in aqueous media. Therefore, the examination of the effect of solution pH on degradation process is of great importance. The effect of the initial pH values and NB concentrations on the degradation of NB has been demonstrated in Fig. 6a. The maximum removal of NB was observed at pH 2 and NB concentration of 40 mg/l (Fig. 6a). A sharp decline happened in the removal of NB with an increase in solution pH from 2.0 to 10, indicating that the reduction of NB using PANI/NZVI CNFs is more favored in acidic conditions. Furthermore, the results can be justified via the reasons below.

At acidic conditions, because of the presence of high amount of reductive factors such as hydrogen ions (H+), the surface corrosion of iron particles will happen. The lower pH values have an undeniable effect on the acceleration of the corrosion of iron and also decrease the amount of iron hydroxide passivated layer onto the surfaces of the modified NZVI which leads to the production of new reactive surface sites [39,40]. However, at alkaline conditions, the production of ferrous hydroxide layer onto the surfaces of NZVI can be enhanced which prevents the reaction of NZVI with contaminants thereby declining transfer of electron and proton to the target pollutant molecules [41]. Removal of NB declined at pH > 2, which can be described via the following phenomena. At isoelectric point (IEP), the surface charge is neutral, which the pH_{IEP} value was determined as 3–4 for PANI/NZVI CNFs (data not shown). The net surface charge at pH values higher and lower than IEP are positive and negative, respectively. Due to the non-ionizable feature of NB, the maximum NB adsorption efficiency happened at pH_{IEP}, which the surface charges of PANI/NZVI CNFs are in neutral states improving the adsorption process. Similar results were also reported for the adsorption of NB onto single-walled carbon nanotubes by Nazari et al. (2013) and Mehrizad et al. (2016) [11,42]. Therefore, the optimum pH value for the degradation of NB using PANI/NZVI CNFs was 2.0. According to the influence of solution pH on the reaction, it can be postulated that the inducing reaction at acidic conditions is important to remove NB from aqueous solutions [43]. Similar findings are present in the literature, for instance, based on the results reported by Yin et al. (2012) in NB reduction by NZVI, acidic conditions were favorable to the p-ClNB removal and also an increase in the initial groundwater pH (3.0–11.0) the rate of p-ClNB degradation decreased [44]. The effect of pH on the reductive removal of NB using Iron NPs immobilized in PEG/nylon membrane showed NB removal has increasing trend with decreasing pH of solution (Tong 2011)[17]. Mu et al. (2004) reported a similar trend in terms of dependency of solution pH with NB reductive removal in aqueous media using zerovalent iron [45]. Fig. 6b illustrates the effect of initial NB concentrations and CNFs dosages on the degradation efficiency. The maximum removal efficiency of NB was observed at CNF dosage of 1.5 g/L and initial NB concentration of 40 mg/L, as shown in Fig. 6b. The results also indicated that the degradation percentage was inversely proportional to the initial NB concentrations and the NB removal experienced a decreasing trend with an enhancement in initial NB concentrations from 40 to 200 mg/L. Such phenomenon can be ascribed to the constant number of surface reactive sites on the PANI/NZVI CNFs against increasing NB concentration. Indeed, NB degradation by means of PANI/NZVI CNFs was a two-step process containing NB sorption onto the surfaces of PANI/NZVI CNFs, which was followed by reduction [41]. The results were consistent with other studies reporting that the NB degradation decreased with increasing initial NB concentrations. For example, Li et al. (2016) stated that an increase in NB initial concentration led to a decrease in removal efficiency, because of the limitation of the adsorption capacity and reaction site on Hangjin clay supported nZVI (HJ-nZVI) [46]. Duan et al., who studied the nitrobenzene degradation by Fenton-like reaction in a H_2O_2/schwertmannite system, reported similar observations [33]. Also, Bia et al. (2017) investigated NB degradation by the Fenton process and they concluded that increasing initial NB concentrations had a negative effect on the initial reaction of Fenton process which, in turn, decreased the removal efficiency [4].

Mehrizad et al. (2016) stated that the removal percentage of 1-Chloro-4-Nitrobenzene (1C4NB) by carbon nanofiber decreased with raising the initial concentration of 1C4NB which can be ascribed to this phenomenon that the adsorbent has a limited number of active sites saturated in a certain concentration; as a result, the saturated adsorbent would not be able to uptake more 1C4NB molecules [29].

The effect of pH and PANI/NZVI CNF_s dosage on NB removal has been presented in Fig. 6c. The maximum removal efficiency was achieved at pH 2 and higher amount of PANI/NZVI CNFs (1.5 g/L) (Fig. 6c). The findings also showed that NB removal represent an enhancement with increasing the amount of PANI/NZVI CNFs up to 0.88 g/l; and, at further dosages, the slope of the graph increased slightly. This increase in removal efficiency was due to the availability of greater surface area and adsorption sites for the constant number of NB molecules [41]. Thus, it can be said that the higher dosage of PANI/NZVI CNFs supplies higher surface reactive sites improving the efficiency of PANI/NZVI CNFs for removing further NB from aqueous solution [6,44]. It was found that NB degradation rate showed a significant correlation with the number of surface reactive sites [33]. In general, the excessive iron quantities may lead to the simultaneous enhancement in NB removal and dissolved iron in the solution. Hence, the extreme dosages of iron require further treatment, before being discharged into drinking water resources [2]. Furthermore, NB removal rate did not show a significant enhancement by increasing the content of iron from 0.88 to 1.5 g/L. It is obvious that the required surface reactive sites for NB reductive removal was overloaded and

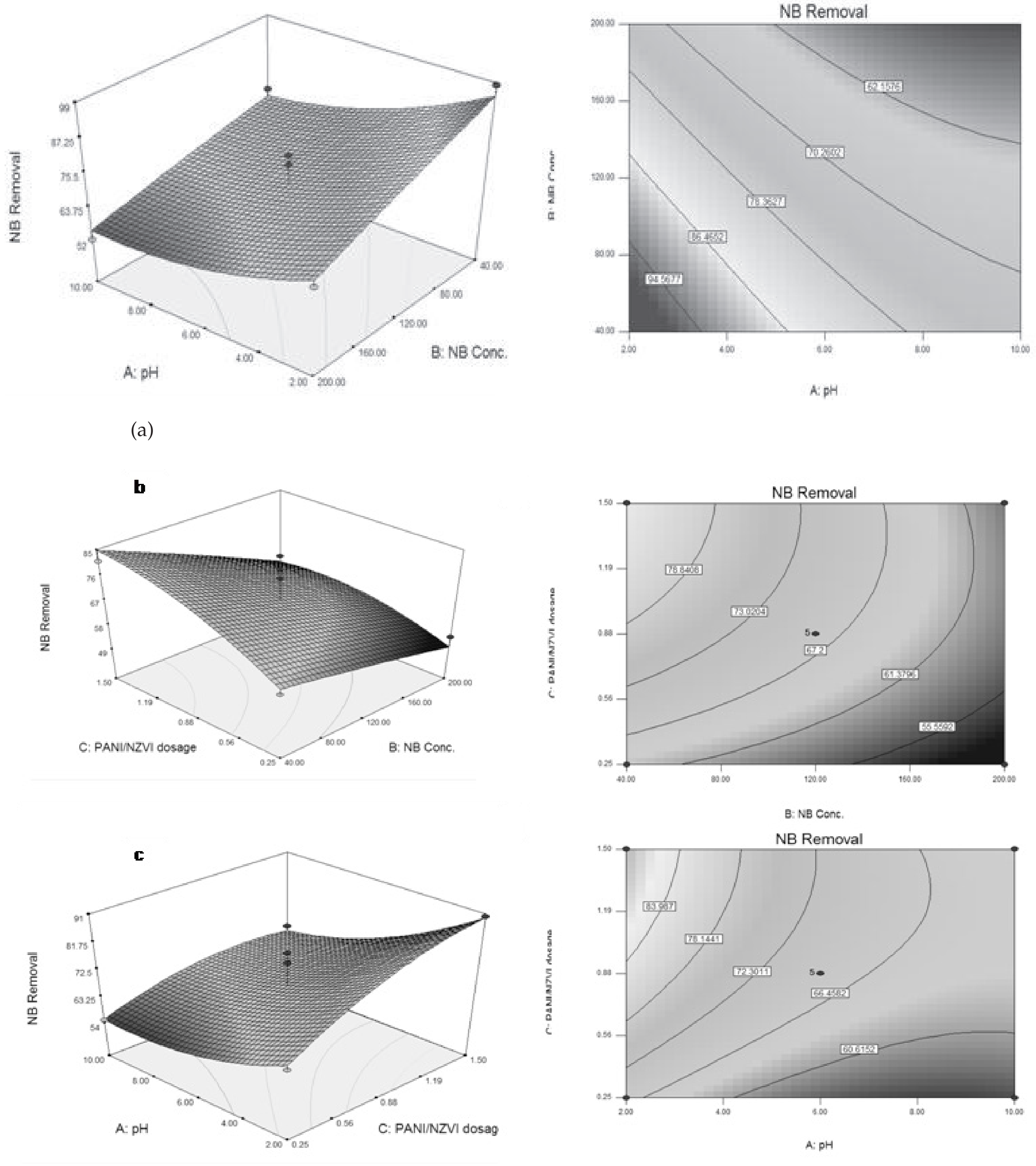

Fig. 6. Effect of operational variables (a) effect of pH and NB concentration (mg/l) on NB removal (time: 45 min and PANI/NZVI CNFs dosage: 0.88 g/l), (b) effect of PANI/NZVI CNFs dosage (g/l) and NB concentration (mg/l) on NB removal (time: 45 min and pH:6) and (c) effect of PANI/NZVI CNFs dosage (g/l) and pH on NB removal (time: 45 min and NB concentration 120 mg/l).

other agents like transport of NB from solution to NZVI surface may restrict the reaction [44]. The research by Li et al. (2014), who studied the removal of p-chloronitrobenzene the (p-ClNB) by NZVI, represented that an enhancement in the quantity of NZVI from 0 to 358.4 mg/L caused p-ClNB removal to improve; the corresponding pseudo-first-order rate constants for p-ClNB degradation increased from 0.01 to 0.18 min^{-1}, which can be attributed to the increasing number of surface reactive sites for H_2O_2 decomposition and creation of higher amounts of reactive oxidants like hydroxyl radicals [32]. In reductive transformation of pentachloro nitrobenzene (p-CNB) by zero-valent iron and mixed anaerobic culture by Yin et al. (2012), the p-CNB degradation efficiency increased from 26.9 to 92.2% with increasing the iron dosage from 0 to

3.0 g L^{-1}. An enhancement in the amount of iron may lead to providing more reactive sites for p-CNB reductive removal using Fe^0 and higher hydrogen production for the biotransformation of p-CNB in the bio-iron system [47]. Duan et al. (2016), who studied NB removal using Fenton-like reaction in a H_2O_2/schwertmannite process, found a direct relationship between NB degradation rate and amount of schwertmannite. The findings showed that NB removal was considerably affected by enhancement of the number of surface reactive sites, which remained unsaturated during Fenton reaction for H_2O_2 decomposition [33]. Based on the ANOVA results (Table 3), a high value of F and low value of P demonstrate a significant interaction between $X_1$and X_2 (pH – initial NB concentration). Fig. 3 shows the 3-D surface and contour plots of the interaction between two factors by holding all the other factors at fixed levels. Therefore, Fig. 3a shows the contour plot and 3-D surface for X_1 (pH) versus X_2 (initial NB concentration). To achieve the removal efficiency more than 95%, as the initial pH value was raised from 10 to 2, the initial concentration of NB should be raised accordingly from 200 to 40 mg/L.

4.4. Process optimization

The optimization process of input variables was performed via the maximization of removal percentage of NB at a specific range of factors. Indeed, the developed quadratic model for the removal percentage of NB (Eq. (5)) was applied as an objective function for finding the optimum operational conditions. As a result, the optimum experimental factors were calculated by means of the numerical technique built in Design Expert software 7, based on the predicted model and the factors in their critical range as constraints. The numerical optimization discovers a design space via the developed model in the analysis for finding the best factors in order to maximize the reductive removal of NB. Based on the mentioned boundaries for factors in Table1, the maximum degradation rate of NB (98.13%), after 45 min, reaction time was obtained at pH 2.04, initial NB concentration 40.23 mg/l and CNFs dosage 0.9 mg/L. The predicted value of degradation by software with desirability equal to 1 was 98.91% (Table 4) [48].

4.5. Study on reaction kinetics

For the analysis of NB concentration variations versus time, kinetic studies were used. Previous researches have shown that the pseudo first-order kinetic model is potentially a suitable model for describing the reaction rate of the NB degradation using NZVI [11,45]. In this regard, the pseudo first-order kinetic model was examined (Fig. 9a). The results confirmed that the degradation rate of NB by PANI/NZVI CNFs depends on initial NB concentration and PANI/NZVI CNFs dosage. Thus,the pseudo first-order rate constant of NB degradation by PANI/NZVI CNFs can be stated by Eq. (6).

$$r = K\,[NB]^a[PANI/NZVI]^b \tag{6}$$

where, r is the reaction rate for NB degradation, k is either the actual or true rate constant and the exponents a and b are the reaction orders of NB and PANI/NZVI, respectively.

Assuming the constant concentration of PANI/NZVI CNFs, Eq. (6) changes as follows:

$$r = k[NB]^a[PANI/NZVI]^b = (k[PANI/NZVI]_0^b\,[NB]^a) = k_{obs}[NB]^a \text{ or } r = \frac{dc}{dt} = -k_{obs}c \tag{7}$$

where, r is the reaction rate, c is the NB concentration, k_{obs} is either the observed or apparent first-order rate constant. The integration of Eq. (6) results in Eq. (7).

$$\ln\left(\frac{c}{c_0}\right) = -k_{obs}t \tag{8}$$

where, C_0 is initial NB concentration and t is reaction time. Therefore, the observed first-order rate constant can be calculated from the slope of the regression line: $\ln(C/C_0)$ versus residence time [1,49]. As shown in Fig. 7a, the fine linear relationship between $\ln(C/C_0)$ and time suggests that the NB reduction reaction with PANI/NZVI CNFs can be expressed in the pseudo first-order kinetic model. The rate constant and regression coefficients of NB reduction by PANI/NZVI CNFs in the pseudo first-order kinetic model are more than those of NZVI. The k_{obs} and R^2 values are 0.009 min^{-1} and 0.805 for NZVI and 0.031 min^{-1} and 0.926 for PANI/NZVI CNFs, respectively. In other words, the reduction rate of PANI/NZVI CNFs is 3.4 times more than that of NZVI, which means that PANI/NZVI CNFs has higher reactivity. We studied NB degradation efficiency from aqueous solution using PANI NFs, NZVI and PANI/NZVI CNFs under the optimum conditions: pH 2, NB concentration 40 mg/L and CNFs dosage 0.88 g/l at different time intervals and the obtained findings have been presented in Fig. 7b. According to Fig. 7, NB degradation efficiency by PANI NFs, NZVI and PANI/NZVI CNFs shows that within the first 45 min of the reaction, almost 92% of NB were removed by PANI/NZVI CNFs, whereas about 63 and 8.4% of NB were removed using NZVI and PANI NFs, respectively [23]. It is noteworthy to mention that after around 10 min, a significant enhancement happened in NB removal efficiency using PANI/NZVI CNFs. This can be attributed to the binding of NB to PANI via the adsorption process. It can be considered as a most effective facet of supporting NZVI on PANI NFs surfaces which caused an increase in the reaction between the adsorbate molecules and the reactive surfaces of NZVI. Furthermore, when PANI NFs containing high surface area come in the NZVI nanoparticle matrix, these substances can act as the excellent support materials, thereby decreasing NZVI nanoparticle agglomeration and not damaging their high activity. Hence, it can be postulated that PANI NFs in PANI/NZVI CNFs system act as a degradant of NB and dispersant of NZVI nanoparticles; it confirms that NB degradation by means of PANI/NZVI CNFs was performed via simultaneous adsorption and reduction processes [23]. In the study by Padervand et al. (2017) research, the results indicated that the photocatalytic reduction of NB can be described by the first-order kinetic model [50]. According to the results reported by Zhang et al. (2016), the photocatalytic degradation of NB in the rotating annular reactor follows the first-order reaction [51]. In another study by Dong et al. (2015), NB reduction by EZVI (emulsified nano-zero-valent iron) and NZVI could be described using the pseudo first-order kinetic model [1].

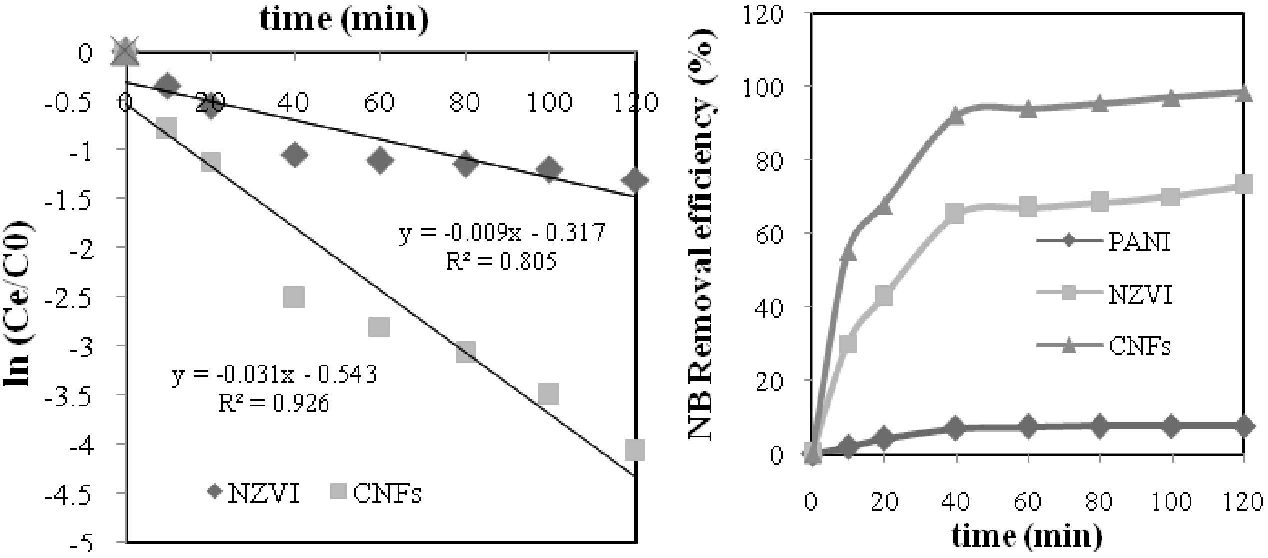

(a) (b)

Fig. 7a. Kinetic model of NB reduction with NZVI and PANI/NZVI CNFs NB concentration and b. comparison of NB removal efficiencies using with PANI NFs, NZVI And PANI/ NZVI CNFs (dose 0.88 g/L, pH 2 and initial NB concentration 40 mg/L).

4.6. Reusability and stability studies

The reusability and stability of remediation agents have always been considered as essential priorities in their application. Based on Fig. 8, for 40 mg/L NB solution, CNFs represent the extensive NB degradation in the first three cycles from 96 to 86%, followed by 81 and 75% in the fourth and fifth cycles. A slight decline in NB degradation rate in the fifth cycle may be because of the abundance of hydroxyl ions and dissolved oxygen that interacted with iron metal ions and, in turn, created iron oxide and hydroxide on their surfaces [12]. The ferrous hydroxides were leached from PANI/NZVI CNFs surface which increased the risk of higher attacks to the adsorbents internal layers that not only resulted in a decrease in the amount of iron in PANI/NZVI CNFs, which was seen via reducing total mass of iron in PANI/NZVI CNFs after each removal cycle, but also decreased NB reductive removal rate. Moreover, a decrease in the reductive removal rate in each cycle would be due to the destruction of nanofibers-like structure of the composite which led to a decline in PANI/NZVI CNFs surface area and simultaneous reduction of NB degradation rate [23].The presence of iron oxide ions acts as a cover on the surfaces of NZVI which either hamper or decline their quick oxidation by means of air or water. Therefore, PANI/NZVI CNFs have the capability of being reused for consecutive cycles without a quick decrease in their high reactivity [46]. Leachate of ingredients from PANI/NZVI CNFs to aqueous environment would lead to secondary pollution. In this case, PANI/NZVI CNFs stability was appraised via measuring the amount of leached Fe. Thus, PANI/NZVI CNFs were washed at different solution pHs: acidic, neutral and basic [52]. According to Fig. 9, a higher amount of iron leaching was observed in acidic conditions compared to neutral or basic solutions (Fig. 9). Generally, it is noteworthy to point that iron leaching can be ignored and was less than the amount of the WHO recommendation for Fe in potable water (0.3 mg L^{-1}) in the pH range of 2 and 12. Due to the high stability of iron on the surface of PANI/NZVI CNFs, the nanocomposite represented extensive magnetic sensitivity by an external magnet. Ai et al. proved that the coverage of PANI/NZVI CNFs surfaces via a protecting layer is an effective approach for preventing iron leaching from Fe_3O_4,which indicates the high magnetic sensitivity of PANI/NZVI CNFs [53].

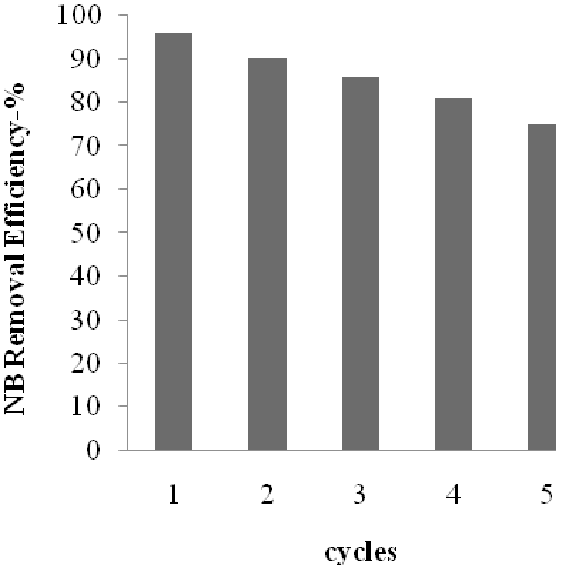

Fig. 8. Sustained reactivity of CNFs for NB reduction (0.88 g L^{-1}, [NB] ini = 40 mg L^{-1}, pH (ini) = 2.0).

4.7. Analysis of reaction products

GC/MS analysis was performed to investigate the main products of NB decomposition by PANI/NZVI CNFs. The reduction of NB by PANI/NZVI CNFs is known to produce aniline, nitrosobenzene, phenyl hydroxylamine, azobenzene and azoxybenzene as the reaction intermediates. In Fig. 11, the probably pathways of reductive degradation of NB by PANI/NZVI CNFs have been shown. Based on the GC/MS analysis results, the mechanism of NB decomposition in the presence of PANI/NZVI CNFs has been proposed (Fig. 10). Hydrated electrons were released from oxidation reaction of NZVI to Fe^{2+}, which resulted in deoxidizing NB to nitrosobenzene. Further reduction of nitrosobenzene produced aniline. Azobenzene, phenyl hydroxylamine and azoxybenzene are generated as a result of the combination of reactive intermediates during the deoxidization processes. In the research by Ling et al. (2012) on reduction of NB by nanoscale zero-valent iron/ordered mesoporous carbon (OMC), the reduction products were as follows: 1-Phenylhydroxylamine, 2-aniline, 3-nitrobenzene, 4-nitrosobenzene [12]. Reductive products of NB decomposition by S-ZVI in GC/MS spectra consisted of aniline, nitrobenzene, azobenzene and azoxybenzene and the reduction of NB by ZVI is known to produce aniline via nitrosobenzene and phenyl hydroxylamine, forming azobenzene and azoxybenzene as reaction intermediates [54].

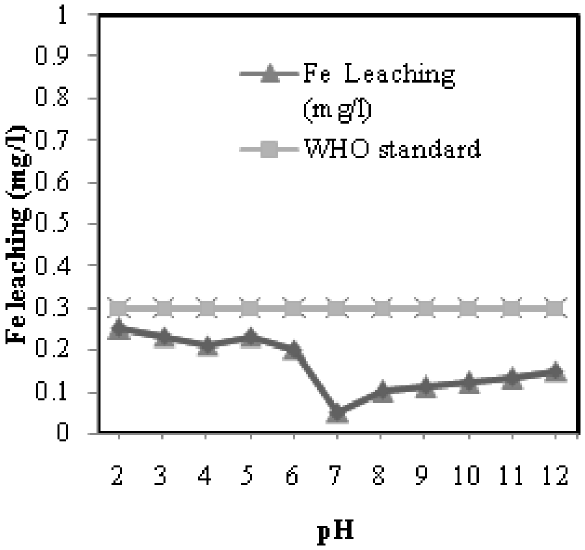

Fig. 9. Tendency of iron leaching under acidic, neutral, and basic conditions.

5. Conclusion

In this research, response surface methodology was applied to optimize the individual and interaction effects of the input variables. The screening experiments revealed that the significant factors in NB removal were pH, initial NB concentration, CNF dosage and interaction between initial NB concentration and PANI/NZVI CNFs dosage. The obtained findings indicated that the removal efficiency represented an increasing trend by an enhancement in PANI/NZVI CNFs dosage and a decrease in initial NB concentration and pH values. The analytical results of GC/MS analysis identified aniline, nitrosobenzene, phenyl hydroxylamine, azobenzene and azoxybenzene as the main intermediate by-products from the NB degradation in the

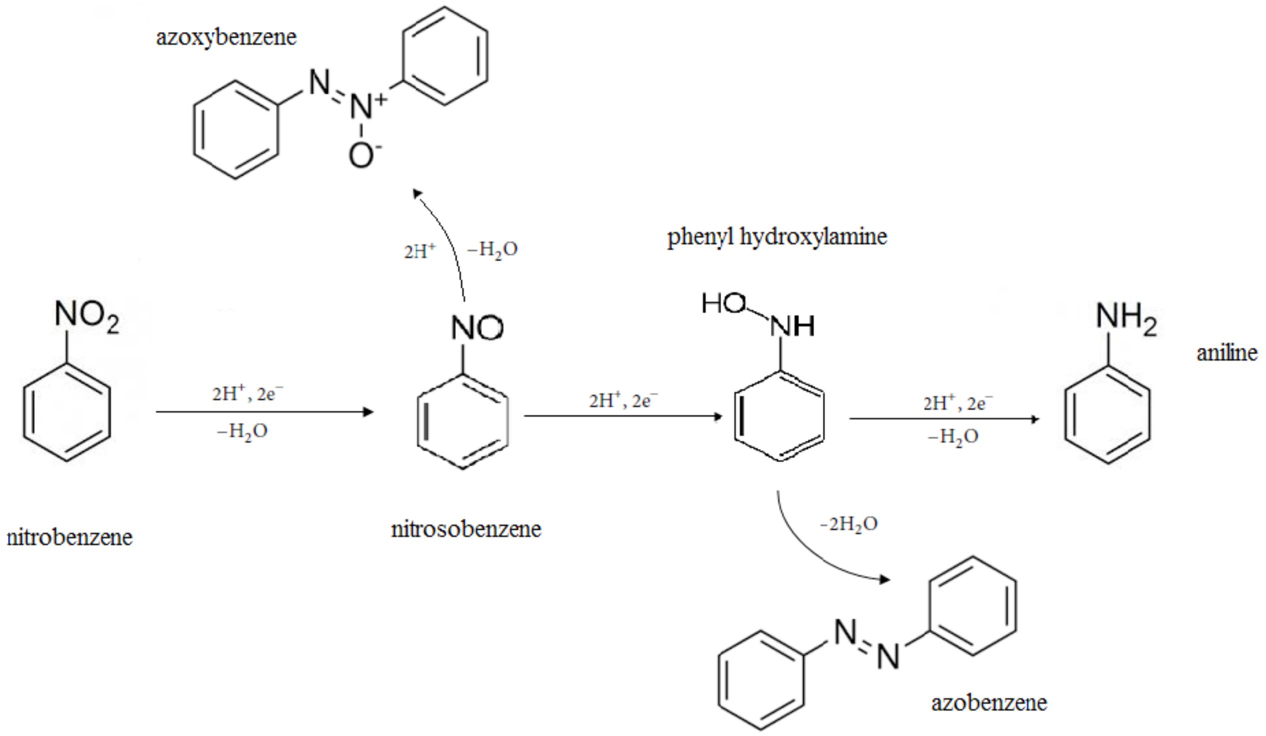

Fig. 10. Probably pathways of NB reductive degradation by PANI/NZVI CNFs.

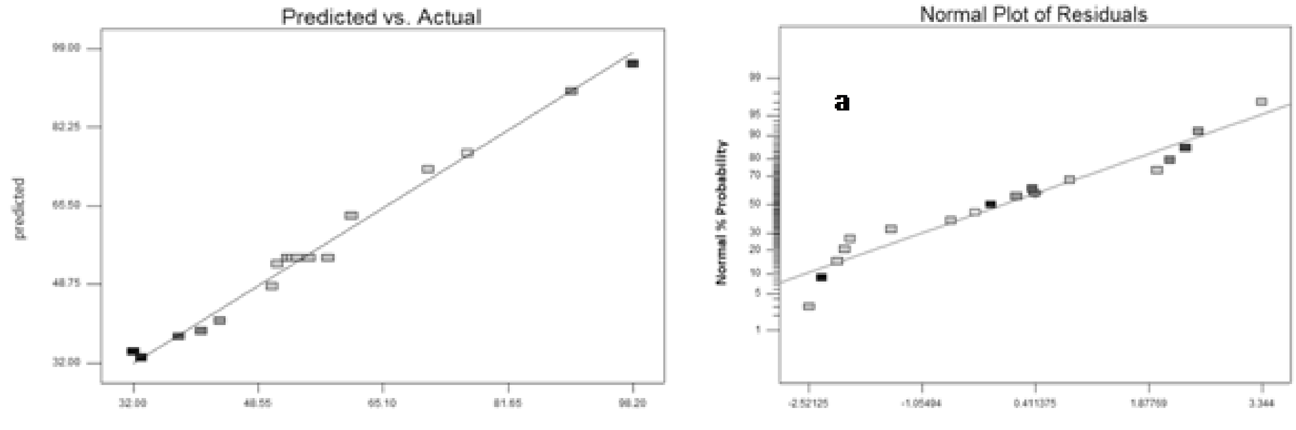

(a) (b)

Fig. 11. Residual plots for Y (efficiency (%)) in the model. (a and b).

PANI/NZVI CNFs system. The ANOVA results confirmed that there was a significant agreement between the predicted and experimental results. It was found that RSM with a Box Behnken design could be considered as an efficient approach to model and optimize the experimental factors.

Conflict of Interests

The authors of this paper express that there is not any conflict of interest.

Acknowledgment

The present study has been obtained from the project No. 94-05-27-27509. Therefore, the authors appreciated from Deputy of Iran University of Medical Sciences for their financial and academic supports.

References:

[1] J. Dong, C. Wen, D. Liu, W. Zhang, J. Li, H. Jiang, et al., Study on degradation of nitrobenzene in groundwater using emulsified nano-zero-valent iron, J. Nanopart. Res., 17 (2015) 1–11.

[2] S. Hu, H. Yao, K. Wang, C. Lu, Y. Wu, Intensify removal of nitrobenzene from aqueous solution using nano-zero valent iron/granular activated carbon composite as fenton-like catalyst, Water Air Soil Pollut., 226 (2015) 1–13.

[3] H. Bai, P. He, J. Pan, J. Chen, Y. Chen, F. Dong, et al., Boron-doped diamond electrode: Preparation, characterization and application for electrocatalytic degradation of m-dinitrobenzene, J. Colloid. Interf. Sci., 497 (2017) 422–428.

[4] J. Bai, Y. Liu, X. Yin, H. Duan, J. Ma, Efficient removal of nitrobenzene by Fenton-like process with Co-Fe layered double hydroxide, Appl. Surf. Sci., 416 (2017) 45–50.

[5] C. Ciou, C. Liang, 1, 3-Dinitrobenzene reductive degradation by alkaline ascorbic acid–Reaction mechanisms, degradation pathways and reagent optimization, Chemosphere, 166 (2017) 482–488.

[6] H. Li, Y.-s. Zhao, R. Zhao, B.-w. Ma, Z.-f. Chen, Y. Su, et al., Characteristics and kinetics of nitrobenzene reduction by sucrose-modified nanoiron, Chem. Res. Chinese U., 29 (2013) 765–770.

[7] S. Jeong, H. Lee, H. Park, K.-J. Jeon, Y.-K. Park, S.-C. Jung, Rapid photocatalytic degradation of nitrobenzene under the simultaneous illumination of UV and microwave radiation fields with a TiO_2 ball catalyst, Catal. Today., 307 (2018) 65–72.

[8] D. Gu, N. Shao, Y. Zhu, H. Wu, B. Wang, Solar-driven thermo-and electrochemical degradation of nitrobenzene in wastewater: Adaptation and adoption of solar STEP concept, J. Hazard. Mater., 321 (2017) 703–710.

[9] W. Jiao, Y. Qin, S. Luo, Z. He, Z. Feng, Y. Liu, Simultaneous formation of nanoscale zero-valent iron and degradation of nitrobenzene in wastewater in an impinging stream-rotating packed bed reactor, Chem. Eng. J., 321 (2017) 564–571.

[10] C. Ren, Y. Li, J. Li, G. Sheng, L. Hu, X. Zheng, Immobilization of nanoscale zero valent iron on organobentonite for accelerated reduction of nitrobenzene, J. Chem. Technol. Biotechnol., 89 (2014) 1961–1966.

[11] A. Mehrizad, P. Gharbani. Study of 1-Chloro-4-Nitrobenzene adsorption on Carbon nanofibers by experimental design, Int. J. Nano. Dimen., 7 (2016) 77–84.

[12] X. Ling, J. Li, W. Zhu, Y. Zhu, X. Sun, J. Shen, et al., Synthesis of nanoscale zero-valent iron/ordered mesoporous carbon for adsorption and synergistic reduction of nitrobenzene, Chemosphere. 87 (2012) 655–660.

[13] R. Zhang, J. Li, C. Liu, J. Shen, X. Sun, W. Han, et al., Reduction of nitrobenzene using nanoscale zero-valent iron confined in channels of ordered mesoporous silica, Colloids. Surf. A. Physicochem. Eng. Asp., 425 (2013) 108–114.

[14] M. Naushad, T. Ahamad, B.M. Al-Maswari, A.A. Alqadami, S.M. Alshehri, Nickel ferrite bearing nitrogen-doped mesoporous carbon as efficient adsorbent for the removal of highly toxic metal ion from aqueous medium, Chem. Eng. J., 330 (2017) 1351–1360.

[15] X. Peng, X. Liu, Y. Zhou, B. Peng, L. Tang, L. Luo, et al., New insights into the activity of a biochar supported nanoscale zerovalent iron composite and nanoscale zero valent iron under anaerobic or aerobic conditions, RSC Adv., 7 (2017) 8755–8761.

[16] L. Tang, J. Tang, G. Zeng, G. Yang, X. Xie, Y. Zhou, et al., Rapid reductive degradation of aqueous p-nitrophenol using nanoscale zero-valent iron particles immobilized on mesoporous silica with enhanced antioxidation effect, Appl. Surf Sci., 333 (2015) 220–228.

[17] M. Tong, S. Yuan, H. Long, M. Zheng, L. Wang, J. Chen, Reduction of nitrobenzene in groundwater by iron nanoparticles immobilized in PEG/nylon membrane, J. Contam. Hydrol., 122 (2011) 16–25.

[18] M. Bhaumik, H.J. Choi, R.I. McCrindle, A. Maity, Composite nanofibers prepared from metallic iron nanoparticles and polyaniline: High performance for water treatment applications, J. Colloid. Interf. Sci., 425 (2014) 75–82.

[19] D. Pathania, G. Sharma, A. Kumar, M. Naushad, S. Kalia, A. Sharma, et al., Combined sorptional–photocatalytic remediation of dyes by polyaniline Zr (IV) selenotungstophosphate nanocomposite, Toxicol. Environ. Chem., 97 (2015) 526–537.

[20] G. Sharma, M. Naushad, A. Kumar, S. Devi, M.R. Khan, Lanthanum/Cadmium/Polyaniline bimetallic nanocomposite for the photodegradation of organic pollutant, Iran Polym. J., 24 (2015) 1003–1013.

[21] G. Sharma, D. Pathania, M. Naushad, Preparation, characterization, and ion exchange behavior of nanocomposite polyaniline zirconium (IV) selenotungstophosphate for the separation of toxic metal ions, Ionics, 21 (2015) 1045–1055.

[22] M. Naushad, Z. Al-Othman, M. Islam, Adsorption of cadmium ion using a new composite cation-exchanger polyaniline Sn (IV) silicate: kinetics, thermodynamic and isotherm studies, Int. J. Environ. Sci. Technol., 10 (2013) 567–578.

[23] M. Bhaumik, C. Noubactep, V.K. Gupta, R. McCrindle, A. Maity, Polyaniline/Fe^0 composite nanofibers: an excellent adsorbent for the removal of arsenic from aqueous solutions, Chem. Eng. J., 271 (2015) 135–146.

[24] N. Colak, A. Özyilmaz, Polyaniline coating on iron–synthesis and characterization, Polym. Plast. Technol. Eng., 44 (2005) 1547–1558.

[25] X. Yue, Z. Liu, Q. Zhang, X. Li, F. Hao, J. Wei, et al., Oxidative degradation of Rhodamine B in aqueous solution using Fe/PANI nanoparticles in the presence of AQS serving as an electron shuttle, Desal. Water Treat., 57 (2016) 15190–15199.

[26] B.D. Yirsaw, M. Megharaj, Z. Chen, R. Naidu, Reduction of hexavalent chromium by green synthesized nano zero valent iron and process optimization using response surface methodology, Environ. Technol. Innov., 5 (2016) 136–147.

[27] J. Gou, Q. Ma, Y. Cui, X. Deng, H. Zhang, X. Cheng, et al., Visible light photocatalytic removal performance and mechanism of diclofenac degradation by Ag_3PO_4 sub-microcrystals through response surface methodology, J. Ind. Eng. Chem., 49 (2017) 112–121.

[28] H. Aghdasinia, R. Bagheri, B. Vahid, A. Khataee, Central composite design optimization of pilot plant fluidized-bed heterogeneous Fenton process for degradation of an azo dye, Environ. Technol., (2016) 1–10.

[29] N. Sivarajasekar, K. Balasubramani, N. Mohanraj, J.P. Maran, S. Sivamani, P.A. Koya, et al., Fixed-bed adsorption of atrazine onto microwave irradiated Aegle marmelos Correa fruit shell: Statistical optimization, process design and breakthrough modeling, J. Mol. Liq., 241 (2017) 823–830.

[30] B. Desalegn, M. Megharaj, Z. Chen, R. Naidu, Reduction of hexavalent chromium by green synthesized nano zero valent iron and process optimization using response surface methodology, Environ. Technol. Innov., 5 (2016) 136–147.

[31] W. Guo, F. Hao, X. Yue, Z. Liu, Q. Zhang, X. Li, et al., Rhodamine B removal using polyaniline-supported zero-valent iron powder in the presence of dissolved oxygen, Environ. Prog. Sustain. Energy, 35 (2016) 48–55.

[32] B. Li, J. Zhu, Removal of p-chloronitrobenzene from groundwater: Effectiveness and degradation mechanism of a heterogeneous nanoparticulate zero-valent iron (NZVI)-induced Fenton process, Chem. Eng. J., 255 (2014) 225–232.

[33] H. Duan, Y. Liu, X. Yin, J. Bai, J. Qi, Degradation of nitrobenzene by Fenton-like reaction in a H_2O_2/schwertmannite system, Chem. Eng. J., 283 (2016) 873–879.

[34] J. Dong, C. Wen, D. Liu, W. Zhang, J. Li, H. Jiang, et al., Study on degradation of nitrobenzene in groundwater using emulsified nano-zero-valent iron, J. Nanopart. Res., 17 (2015) 1–11.

[35] S. Sohrabi, F. Akhlaghian, Modeling and optimization of phenol degradation over copper-doped titanium dioxide photocatalyst using response surface methodology, Process. Saf. Environ. Prot., 99 (2016) 120–128.

[36] S.H. Piao, M. Bhaumik, A. Maity, H.J. Choi, Polyaniline/Fe composite nanofiber added softmagnetic carbonyl iron microsphere suspension and its magnetorheology, J. Mater. Chem. C., 3 (2015) 1861–1868.

[37] T. Tatarchuk, N. Paliychuk, M. Bououdina, B. Al-Najar, M. Pacia, W. Macyk, et al., Effect of cobalt substitution on structural, elastic, magnetic and optical properties of zinc ferrite nanoparticles, J. Alloys Compd., 731 (2018) 1256–1266.

[38] T. Tatarchuk, M. Bououdina, N. Paliychuk, I. Yaremiy, V. Moklyak, Structural characterization and antistructure modeling of cobalt-substituted zinc ferrites, J. Alloys Compd., 694 (2017) 777–791.

[39] A. Agrawal, P.G. Tratnyek, Reduction of nitro aromatic compounds by zero-valent iron metal, Environ. Sci. Technol., 30 (1995) 153–160.

[40] J. Dong, Y. Zhao, R. Zhao, R. Zhou, Effects of pH and particle size on kinetics of nitrobenzene reduction by zero-valent iron, J. Environ. Sci., 22 (2010) 1741–1747.

[41] P. SivaKumar, D. Prabhakaran, T. Kannadasan, S. Karthikeyan, Optimization studies on electrochemical and biosorption treatment of effluent containing nitro benzene by RSM, Int. J. Biosci., (IJB) 3 (2013) 1–7.

[42] S. Nazari, P. Gharbani, Adsorption of 1-chloro-4-nitrobenzene from aqueous solutions onto single-walled carbon nanotubes, Int. J. Nano Dimens., 3 (2013) 263–269.

[43] H. Keypour, M. Noroozi, A. Rashidi, M. Shariati Rad, Application of response surface methodology for catalytic hydrogenation of nitrobenzene to aniline using ruthenium supported fullerene nanocatalyst, Iran J. Chem. Eng., 34 (2015) 21–32.

[44] W. Yin, J. Wu, P. Li, X. Wang, N. Zhu, P. Wu, et al., Experimental study of zero-valent iron induced nitrobenzene reduction in groundwater: the effects of pH, iron dosage, oxygen and common dissolved anions, Chem. Eng. J., 184 (2012) 198–204.

[45] Y. Mu, H.-Q. Yu, J.-C. Zheng, S.-J. Zhang, G.-P. Sheng, Reductive degradation of nitrobenzene in aqueous solution by zero-valent iron, Chemosphere, 54 (2004) 789–794.

[46] X. Li, Y. Zhao, B. Xi, X. Mao, B. Gong, R. Li, et al., Removal of nitrobenzene by immobilized nanoscale zero-valent iron: Effect of clay support and efficiency optimization, Appl. Surf. Sci., 370 (2016) 260–269.

[47] W. Yin, J. Wu, P. Li, G. Lin, X. Wang, B. Zhu, et al., Reductive transformation of pentachloronitrobenzene by zero-valent iron and mixed anaerobic culture, Chem. Eng. J., 210 (2012) 309–315.

[48] M. Vaez, A. Zarringhalam Moghaddam, S. Alijani, Optimization and modeling of photocatalytic degradation of azo dye using a response surface methodology (RSM) based on the central composite design with immobilized titania nanoparticles, Ind. Eng. Chem. Res., 51 (2012) 4199–4207.

[49] C. Liang, Y.-T. Lin, J.-W. Shiu, Reduction of nitrobenzene with alkaline ascorbic acid: kinetics and pathways, J. Hazard Mater., 302 (2016) 137–143.

[50] M. Padervand, A. Rahmani, S. Rahimnejad, M.R. Gholami, Highly efficient nitrobenzene photoreduction over the amino acid-modified CdS-TiO_2 nanostructures under visible light, Nanochem. Res., 2 (2017) 109–119.

[51] S. Zhang, L. Li, Y. Liu, Q. Zhang, TiO_2-SA-Arg nanoparticles stabilized pickering emulsion for photocatalytic degradation of nitrobenzene in a rotating annular reactor, Chin. J. Chem. Eng., (2016).

[52] R. Rezaei Kalantary, A. Azari, A. Esrafili, K. Yaghmaeian, M. Moradi, K. Sharafi, The survey of Malathion removal using magnetic graphene oxide nanocomposite as a novel adsorbent: thermodynamics, isotherms, and kinetic study, Desal. Water Treat., 57 (2016) 28460–28473.

[53] L. Ai, Y. Zhou, J. Jiang, Removal of methylene blue from aqueous solution by montmorillonite/$CoFe_2O_4$ composite with magnetic separation performance, Desalination, 266 (2011) 72–77.

[54] H. Lee, B.-H. Kim, Y.-K. Park, S.-J. Kim, S.-C. Jung, Application of recycled zero-valent iron nanoparticle to the treatment of wastewater containing nitrobenzene, J. Nanomate., 16 (2015) 363–375.